Journal of Advanced Mechanical Design, Systems, and Manufacturing

Vol. 7, No. 4, 2013

Recess Design and Dynamic Control of an Active Compensating Hydrostatic Bearing*

Ming-Chang SHIH** and Jen-Sheng SHIE**

** Department of mechanical Engineering, National Cheng-Kung University

701 Tainan City, Taiwan, R.O.C.

E-mail:mcshih@mail.ncku.edu.tw

Abstract

This paper describes the optimum design of recess shape for the proposed hydrostatic bearing, and dynamic control of oil film thickness for an active compensating hydrostatic bearing by using a servo valve and a proposed controller. First of all, this study is theoretical study concerning static performance of a hydrostatic bearing having recess of optimal shape parameters. Because of the recess of the traditional hydrostatic bearing only has one oil outlet that is easy to concentrate the pressure of the recess at the outlet, leading to non-uniform pressure distribution. Hence, the objectives of this study are to design a hydrostatic bearing with high load capacity, high stiffness, low flow rate and uniform pressure distribution by using HTGA/Gray optimal approach. In addition, this study integrates servo control technology to compensate the pressure of the bearing with an intelligent nonlinear controller to maintain a constant oil film thickness. However, the hydrostatic bearing is a nonlinear system and is affected by numerous uncertainties; that is, the parameters can be changed by factors, such as temperature, leakage, and disturbance. Therefore, the proposed controller proposes a self-tuning mechanism to modify the output scaling factor, and adds a dead zone compensator to avoid the insensitive area of a servo valve. Finally, the experimental results are used to verify the feasibility and practicality of this study.

Key words: Hydrostatic Bearing, Optimal Design, Dynamic Control, Self-Tuning Fuzzy Sliding Mode Controller, Dead Zone Compensator

1. Introduction

Hydrostatic bearings have been widely applied in high-precision mechanisms because of their qualities, including substantially low friction, high stiffness, high accuracy, and long service life. However, the performance of bearings is greatly affected by the recess shape during the design process and the type of restrictor. A through scan of the literature concerning the hydrostatic bearing indicates that the majority of the studies are a rectangular shape of the recess. This may be because of ease of manufacturing. However, owing to rapid technological advancements in manufacturing techniques, the other recess shapes can now be easily manufactured.

Rowe and O'Donoghue[1), 2)] discusses selection of suitable values for hydrostatic bearing design variables with a view to minimizing power dissipation and reducing the temperature rise. The optimum sill width ratio is 25% when expressed in an appropriate form. Ghosh and Majumdar describe computer generated design data in terms of load capacity and oil flow for multirecess hydrostatic journal bearing[3)]. The Reynolds equation for a finite bearing was solved on a high speed digital computer satisfying appropriate

*Received 7 June, 2013 (No. 13-00091)
[DOI: 10. 1299/jamdsm.7.706]

boundary conditions and using the finite difference method. Results for various L/D ratios, recess to bearing area ratios, number of recesses etc are presented for capillary and orifice restrictor. Franchek and Childs[4] experimentally studied the five oil pockets, high speed, high pressure, orifice compensated hybrid bearings for cryogenic environments such as that in the Space Shuttle Main Engine (SSME). Four hybrid bearings having different geometric configurations were experimentally tested for their static and dynamic characteristics, including flow rate, load capacity etc. Their study reported that a square recess bearing with an aligned orifice had the best performance among all the bearings studied. Sharma et al. studied the static and dynamic performance of a circular thrust pad hydrostatic bearing with circular, rectangular, elliptical and annular recess. The computed results indicate that to get an improved performance from a hydrostatic circular thrust pad bearing, a proper selection of the geometric shape of the recess in conjunction with the type of restrictor and the restrictor design parameter is essential[5]. Sharma and Singh used the third-order polynomial of pressure difference to determine the flow rate of membrane-type restrictor for studying the influences of bearing flexibility and recess shape on the performance characteristics of multirecess journal bearings[6], [7].

Because the precision industry has advanced recently, the demand for accuracy and for products has also been increasing. The traditional machine tool has been losing its ability to meet the requirements. Therefore, a hydrostatic bearing with a compensator has become one of the key components of precision machine tools. This paper proposed that the hydrostatic bearing could be actively compensated for using a hydraulic servo control technology to maintain a constant oil film thickness, unlike the typical compensation range of hydrostatic bearings that are constrained by the stiffness of adjusting mechanism, such as membrane-type and spool-type[8]-[13]. Many studies have employed oil film thickness control for a controllable hydrostatic bearing. Hesselbach and Abel-keilhack[14] present a hydrostatic bearing that uses magnetorheological fluids. Due to the fact that magnetorheological fluids change their rheological properties with the change of an external magnetic field, it is possible to achieve a constant bearing gap even if the payload changes. Munzinger et al. describe a smart adaptronic hydrostatic guiding system for machine tool slides. The use of smart piezoelectric transducers for higher frequency excitations in order to reduce vibrations[15]. J. Shao et al. presents a controllable hydrostatic bearing to improve rigidity. The worktable poses were controlled by coupling oil film thickness of four controllable chambers. The chamber flow can be regulated by electro hydraulic servo valve control variable pump and using the hardware-in-loop simulation experiment was carried out on the servo test bench[16].

2. Modeling of a hydrostatic bearing

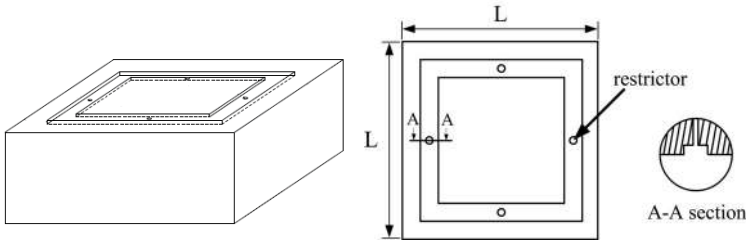

Fig. 1 The geometry of a square hydrostatic bearing with □-shaped recess

Figure 1 shows the proposed design of a square hydrostatic bearing with □-shaped recess is shown as Fig.1. Some basic assumptions are applied in this study before deriving the equation of the hydrostatic bearing. Consider a steady, we assume that the fluid properties are isotropic, incompressible and isoviscous. The governing equations for this

problem can be written as follows:

$$\begin{cases} \partial p/\partial x = \mu\left(\partial^2 u/\partial z^2\right) \\ \partial p/\partial y = \mu\left(\partial^2 v/\partial z^2\right) \\ \partial p/\partial z = 0 \end{cases} \tag{1}$$

where p is the pressure distribution of the bearing, μ is the viscosity of lubricating, u, v and w are three component of the velocity vector respectively along x, y and z axes. Eq. (1) may be integrated twice and evaluated to determine the velocity distribution. The boundary conditions employed are $u=0$ and $v=0$ at $z=0$ or h. The velocity distribution is given by

$$\begin{cases} u = -\dfrac{1}{2\mu}\left(\partial p/\partial x\right)\left(h-z\right)z \\ v = -\dfrac{1}{2\mu}\left(\partial p/\partial y\right)\left(h-z\right)z \end{cases} \tag{2}$$

Figure 2 show the finite difference grid of a square hydrostatic bearing. Consider the reference area bounded by dotted lines. The flow rates Q_i, Q_{i+1}, Q_j, Q_{j+1} of the reference area can be written as follows:

$$\begin{cases} Q_i = -h^3/12\mu\cdot\left[\left(P_{i,j}-P_{i-1,j}\right)/\Delta x\right]\Delta y \\ Q_{i+1} = -h^3/12\mu\cdot\left[\left(P_{i+1,j}-P_{i,j}\right)/\Delta x\right]\Delta y \\ Q_j = -h^3/12\mu\cdot\left[\left(P_{i,j}-P_{i,j-1}\right)/\Delta y\right]\Delta x \\ Q_{j+1} = -h^3/12\mu\cdot\left[\left(P_{i,j+1}-P_{i,j}\right)/\Delta y\right]\Delta x \end{cases} \tag{3}$$

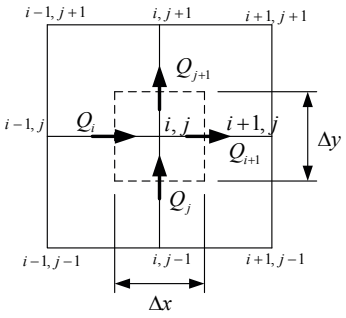

Fig. 2 Finite difference grid of a square hydrostatic bearing

where h is oil film thickness, The continuity equation can be described as

$$Q_i + Q_j - Q_{i+1} - Q_{j+1} = 0 \tag{4}$$

Substituting Eq. (3) into Eq. (4) and then rearranging them, we can describe as

$$P_{i,j} = \frac{A_1 P_{i-1,j} + A_2 P_{i+1,j} + A_3 P_{i,j-1} + A_4 P_{i,j+1}}{A_1 + A_2 + A_3 + A_4} \tag{5}$$

where $A_1 = A_2 = \Delta y h^3/\Delta x$ and $A_3 = A_4 = \Delta x h^3/\Delta y$

Figure 3 show the hydrostatic bearing with recess along x axis. The flow rates Q_i, Q_{i+1}, Q_j, and Q_{j+1} of the reference area can be written as follows:

$$\begin{cases} Q_i = -h^3/12\mu \cdot \left[\left(P_{i,j} - P_{i-1,j} \right)/\Delta x \right] \left[\left(\Delta y - \Delta R_W \right) h^3 + \Delta R_W \left(h + R_H \right)^3 \right] \\ Q_{i+1} = -h^3/12\mu \cdot \left[\left(P_{i+1,j} - P_{i,j} \right)/\Delta x \right] \left[\left(\Delta y - \Delta R_W \right) h^3 + \Delta R_W \left(h + R_H \right)^3 \right] \\ Q_j = -h^3/12\mu \cdot \left[\left(P_{i,j} - P_{i,j-1} \right)/\left(\Delta y - 0.5\Delta R_W \right) \right] \Delta x \\ Q_{j+1} = -h^3/12\mu \cdot \left[\left(P_{i,j+1} - P_{i,j} \right)/\left(\Delta y - 0.5\Delta R_W \right) \right] \Delta x \end{cases} \quad (6)$$

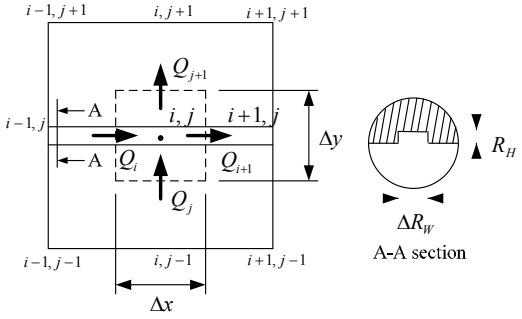

Fig. 3 The hydrostatic bearing with recess along x axis

where R_W is the recess width and G_H is the recess depth. Substituting Eq. (7) into Eq. (5) and then rearranging them, the $P_{i,j}$ can be described as

$$P_{i,j} = \frac{B_1 P_{i-1,j} + B_2 P_{i+1,j} + B_3 P_{i,j-1} + B_4 P_{i,j+1}}{B_1 + B_2 + B_3 + B_4} \quad (7)$$

where

$$B_1 = B_2 = \left[\left(\Delta y - \Delta R_W \right) h^3 + \Delta R_W \left(h + R_H \right)^3 \right] / \Delta x \text{ and } B_3 = B_4 = \Delta x h^3 / \left(\Delta y - 0.5\Delta R_W \right)$$

Figure 4 shows the hydrostatic bearing with recess along x and y axes. According to the flow rate continuity, $P_{i,j}$ can be expressed as

$$P_{i,j} = \frac{C_1 P_{i-1,j} + C_2 P_{i+1,j} + C_3 P_{i,j-1} + C_4 P_{i,j+1}}{C_1 + C_2 + C_3 + C_4} \quad (8)$$

where

$$C_1 = C_2 = \left[\left(\Delta y - \Delta R_W \right) h^3 + \Delta R_W \left(h + R_H \right)^3 \right] / \left(\Delta x - 0.5\Delta R_W \right),$$

$$C_3 = \left[\left(\Delta y - \Delta R_W \right) h^3 + \Delta R_W \left(h + R_H \right)^3 \right] / \left(\Delta y - 0.5\Delta R_W \right), \quad C_4 = \Delta x h^3 / \left(\Delta y - 0.5\Delta R_W \right)$$

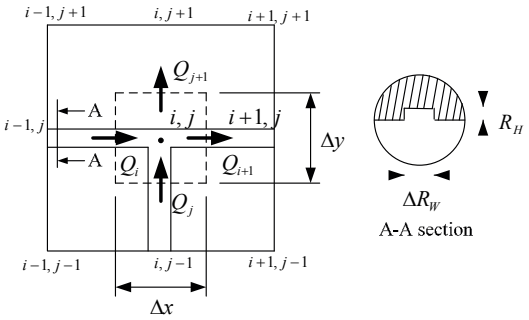

Fig. 4 The hydrostatic bearing with recess along x and y axes

The boundary conditions according to the law of conservation mass to determined the exit pressure from the restrictor, which is the inlet pressure or recess pressure of the bearing. The flow of lubricant through the restrictor is equal to the bearing input flow. It can be presented as

$$Q_{in} = Q_{out} \tag{9}$$

where Q_{in} is the flow rate into the oil film thickness. Q_{out} is the flow rate output from oil film of bearing.

According to the above mathematic model, the pressure distribution can be determined. Therefore, the static performance was obtained for a known value of recess pressure. The static performances of a square hydrostatic bearing includes the load capacity (F), the stiffness (S) and the flow rate (Q) of bearing. Which are expressed as follows:

$$F = \int_0^L \int_0^L p dx dy \tag{10}$$

$$S = \Delta F / \Delta h \tag{11}$$

$$Q = Q_x + Q_y \tag{12}$$

where $Q_x = h^3/12\mu \cdot \int (\partial p/\partial x) dy$ and $Q_y = h^3/12\mu \cdot \int (\partial p/\partial y) dx$

The scheme of the worktable supported by the hydrostatic bearing for the mass-spring-dashpot element is shown in Fig. 5. The equation of the motion of the worktable supported by the hydrostatic bearing can be expressed as

$$M\ddot{h} + C\dot{h} + Sh = W_d - F_d \tag{13}$$

where M is bearing pad and worktalbe mass, $C = -dF/d\dot{h}$ ($\dot{h} = dh/dt$) is the damping coefficient, $S = -dF/dh$ is stiffness coefficient, W_d is regarded as the only external load source, the force $F_d = A_e P_r$, A_e is effective area of bearing, and the controllable pressure u representing P_r. Therefore, the state variables are defined as $x_1 = h$ and $x_2 = \dot{h}$, Hence, the state-space equation can be written as follows

$$\dot{\mathbf{x}}(t) = \mathbf{F}(\mathbf{x}(t)) + \mathbf{B}u(t) + \mathbf{G}W_d(t) \tag{14}$$

where

$$\mathbf{F} = \begin{bmatrix} 0 & 1 \\ -C/M & -S/M \end{bmatrix}, \quad \mathbf{B} = \begin{bmatrix} 0 \\ -A_e/M \end{bmatrix}, \quad \mathbf{G} = \begin{bmatrix} 0 \\ -1/M \end{bmatrix}$$

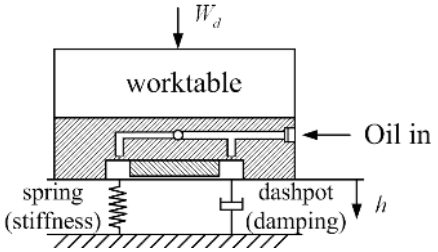

Fig. 5 The single-DOF model of a hydrostatic bearing

3. Optimum recess design for a hydrostatic Bearing

3.1 Static Performance Analysis

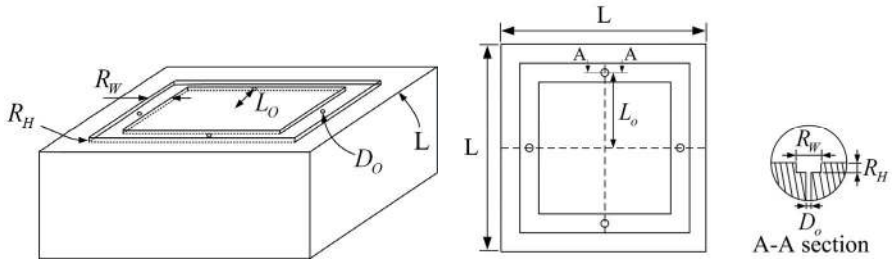

Fig. 6 The proposed parameters of hydrostatic bearing surface recess

Figure 6 shows the schematic diagram of the proposed parameters of hydrostatic bearing surface recess. This section shows the related characteristics of a hydrostatic bearing include the load capacity, stiffness and flow rate of bearing. Fig. 7-10 shows the influence of changes in proposed parameters on each performance. The proposed parameters are given as the orifice location L_O, the orifice diameter D_O, the recess width R_W, and the recess depth R_H. In the Fig. 7-10 (a), it can be seen that when the larger the orifice location, orifice diameter, recess width and depth, the larger the load capacity. The parameters are kept, the larger the film thickness, the smaller the load capacity. In the Fig. 7-10 (b), it can found the stiffness is proportional to film thickness, and the results from these figures are exists a best stiffness between film thickness. In the Fig. 7-10 (c), it can be seen that when the larger the orifice location, orifice diameter, recess width and depth, the larger the flow rate. It will cause energy consumption. The proposed parameters are outstanding effect on performance of bearing such as load capacity, stiffness and flow rate. According to the above information, it can be seen that a set of optimal parameters is exist a best static behavior. Therefore, the objectives of next section are to find the optimal parameters of bearing with high load capacity, high stiffness, low flow rate and uniform pressure distribution.

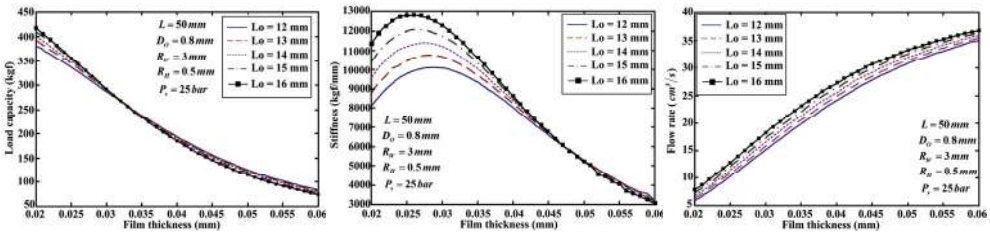

(a) (b) (c)

Fig. 7 Influence of different orifice locations on (a) load capacity, (b) stiffness, and (c) flow rate.

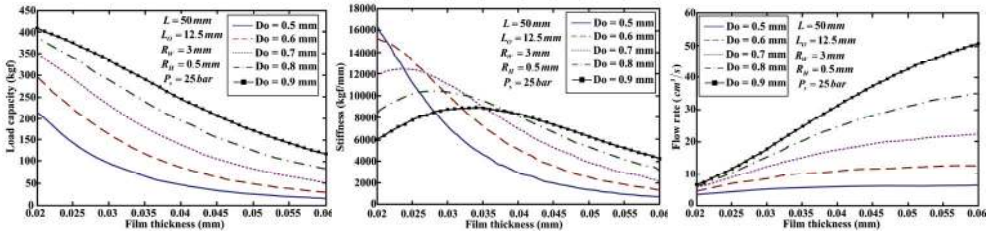

(a) (b) (c)

Fig. 8 Influence of different orifice diameters on (a) load capacity, (b) stiffness, and (c) flow rate.

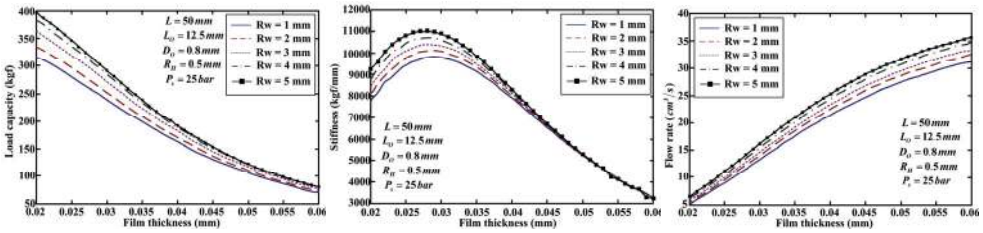

(a) (b) (c)

Fig. 9 Influence of different recess widths on (a) load capacity, (b) stiffness, and (c) flow rate.

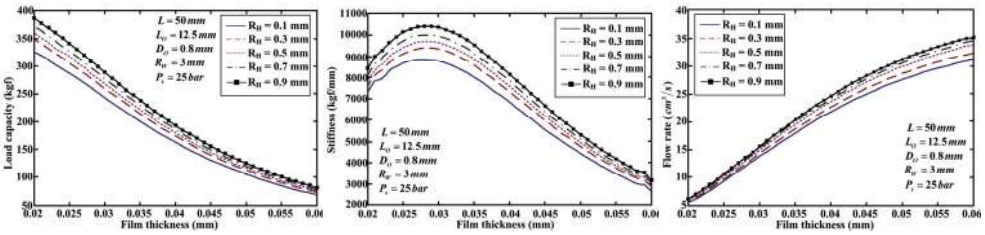

(a) (b) (c)

Fig. 10 Influence of different recess depths on (a) load capacity, (b) stiffness, and (c) flow rate.

3.2 Optimization approach

In this study, the proposed optimization approach is integrated a hybrid Taguchi-Genetic Algorithm (HTGA) and Gray Relational Analysis (GRA) to obtain the optimal parameters of bearing surface recess efficiently. The HTGA combines the genetic algorithm (GA), which has a powerful global exploration capability, with the Taguchi method, which can exploit the optimum offspring. The Taguchi method is inserted between crossover and mutation operations of a GA. Then, the systematic reasoning ability of the Taguchi method is incorporated in the crossover operations to select the better genes to achieve crossover, and consequently, enhance the genetic algorithm. Therefore, the HTGA can be more robust, stability, and quickly convergent[18]. However, the Taguchi method only works for optimization of a single quality characteristic. The gray relational analysis procedure is used to combine all the considered quality characteristics into a single value that can then be used as the single characteristic in optimization problems[19]. The procedure of the proposed HTGA/Gray approach is shown in Fig. 11. In this study, the fitness function is defined as larger as possible, which are consider three capability of a bearing such as load capacity (as larger as possible), stiffness (as larger as possible), and flow rate (as lower as possible) as given by

$$f(L_O, D_O, R_W, R_H) = w_1 F + w_2 S + w_3 (1/Q) + w_4 (F \times S/Q) \tag{15}$$

where w_1 (range of value: 1-10), w_2 (range of value: 0.03-0.3), w_3 (range of value: 40-4000), and w_4 (range of value: 0.001-0.1) are weighting factors. Therefore, according to fitness function of GA and different value of weighting factors, the quality characteristics can be defined as follows:

$$\begin{cases} QC_1 = 0.7w_1 \times F + 0 \times S + 0 \times (1/Q) + 0.3w_4 \times (F \times S)/Q \\ QC_2 = 0 \times F + 0.7w_2 \times S + 0 \times (1/Q) + 0.3w_4 \times (F \times S)/Q \\ QC_3 = 0 \times F + 0 \times S + 0.7w_3 \times (1/Q) + 0.3w_4 \times (F \times S)/Q \end{cases} \tag{16}$$

where QC_1, QC_2 and QC_3 are three types of quality characteristics. According to the above definition, the gray relational generating can be normalized as

$$x_i^*(k)=\frac{x_i(k)-\min_i x_i(k)}{\max_i x_i(k)-\min_i x_i(k)} \tag{17}$$

where $x_i(k)$ is the original sequence, $x_i^*(k)$ is the value after the gray relation generating process, $\min_i x_i(k)$ is the minimum value of $x_i(k)$, and $\max_i x_i(k)$ implies the maximum value of $x_i(k)$. Next, calculate the gray relation grade γ through the following equation

$$\gamma\left(x_0(k),x_i(k)\right)=\frac{\Delta_{min}+\Delta_{max}}{\Delta_{0i}^*(k)+\Delta_{max}},\ 0<\gamma\left(x_0(k),x_i(k)\right)\le 1 \tag{18}$$

$$\Delta_{0i}^*(k)=\frac{1}{n}\sum_{k=1}^{n}\Delta_{0i}(k) \tag{19}$$

where $\Delta_{0i}(k)$ is the deviation sequence of the reference sequence $x_0(k)$ and the comparability sequence $x_i(k)$, $\Delta_{0i}(k)=\left|x_0(k)-x_i(k)\right|$, and Δ_{min}, Δ_{max} are constants as

$$\begin{cases}\Delta_{min}=\forall_i^{min}\in\forall_k^{min}\left|x_0(k)-x_i(k)\right|\\ \Delta_{max}=\forall_i^{max}\in\forall_k^{max}\left|x_0(k)-x_i(k)\right|\end{cases} \tag{20}$$

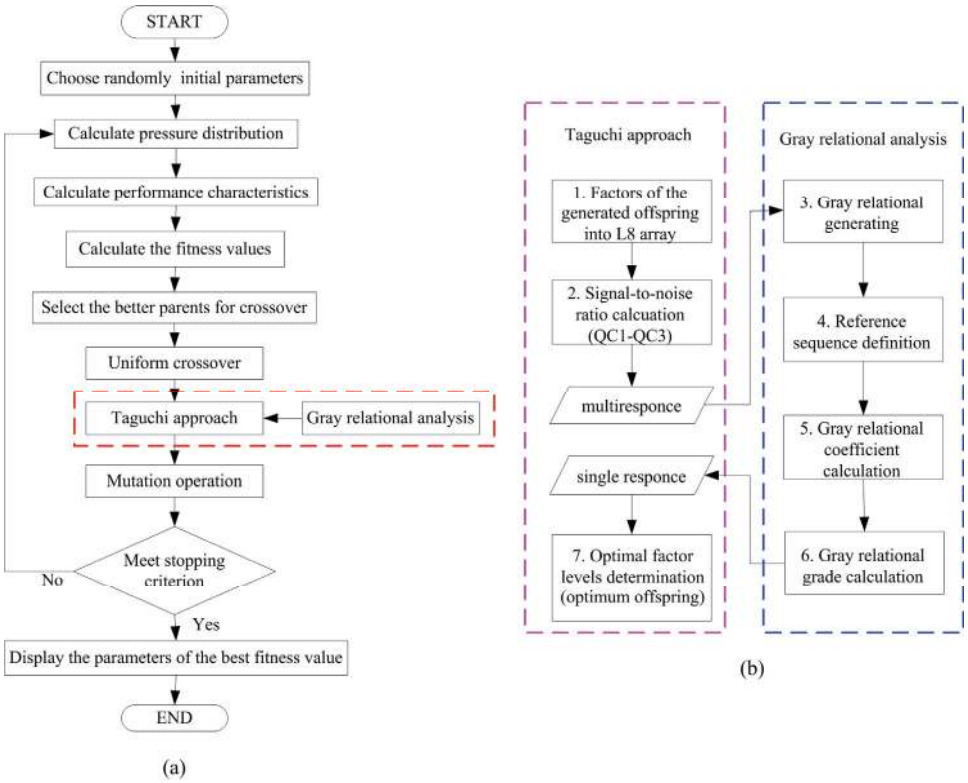

Fig. 11 (a) The flowchart of the HTGA/Gray method (b) procedure of the gray-based Taguchi approach

3.3 Optimum Results

The optimization approach for HTGA/Gray method is used to determine suitable parameters of a hydrostatic bearing for uniform pressure distribution. The result of optimized configuration of the bearing groove as shown in Fig. 12(a). The computer simulation result under constant parameters setting with the supply pressure is 25 bar and

the oil film thickness is 25 μm as shown in Fig. 12(b).

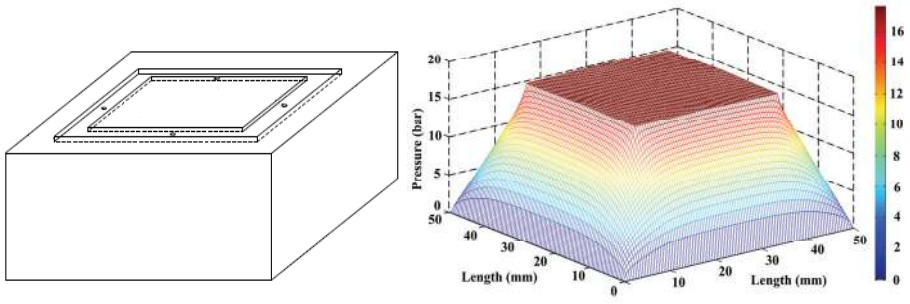

(a) (b)

Fig. 12 (a) The result of optimized configuration of the proposed design. (b) The uniform pressure distribution of a square hydrostatic bearing

The static performance of different supply pressures for the designed hydrostatic bearing as shown in Fig. 13. The following sections compare the performance of the proposed design with referenced hydrostatic bearing[7]. Fig. 14 shows the schematic diagram of the reference hydrostatic bearing. Comparisons were made on the basis of the same supply pressure (25bar) and bearing size (50mm). The comparison results of the bearing performance as shown in Fig. 15. In the Fig. 15, the load capacity and the flow rate of the proposed design are better than referenced hydrostatic bearing, and the stiffness of the proposed design are similar to referenced. It can be seen that the proposed design has a better static performance by using the HTGA/Gray approach.

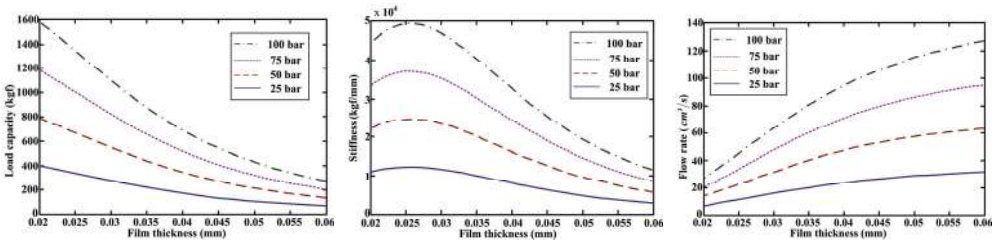

(a) (b) (c)

Fig. 13 The static performances of the different supply pressures (a) load capacities, (b) stiffness, and (c) flow rates

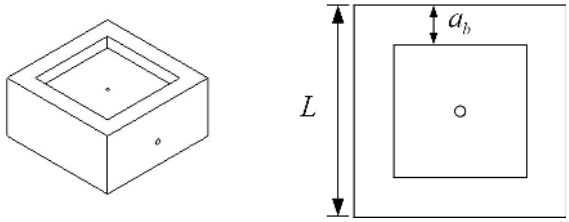

Fig. 14 The recess shape of the referenced hydrostatic bearing for $a_b/L = 0.14$

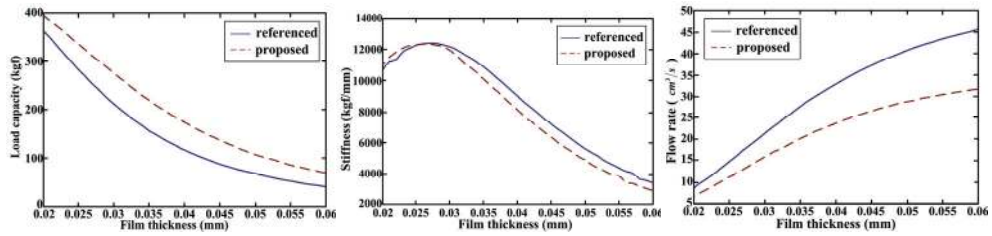

(a) (b) (c)

Fig. 15 The static performance comparison between the referenced and the proposed hydrostatic bearing (a) load capacities, (b) stiffness, and (c) flow rates

After the optimal design of a hydrostatic bearing, the designed bearing has a strong

static performance, but the bearing is that the oil film thickness varies with external load. Therefore, this study proposes a different concept for bearing with servo control technology to active compensating the pressure of the bearing. An intelligent nonlinear controller and dynamic control will present in following section.

4. Controller Design

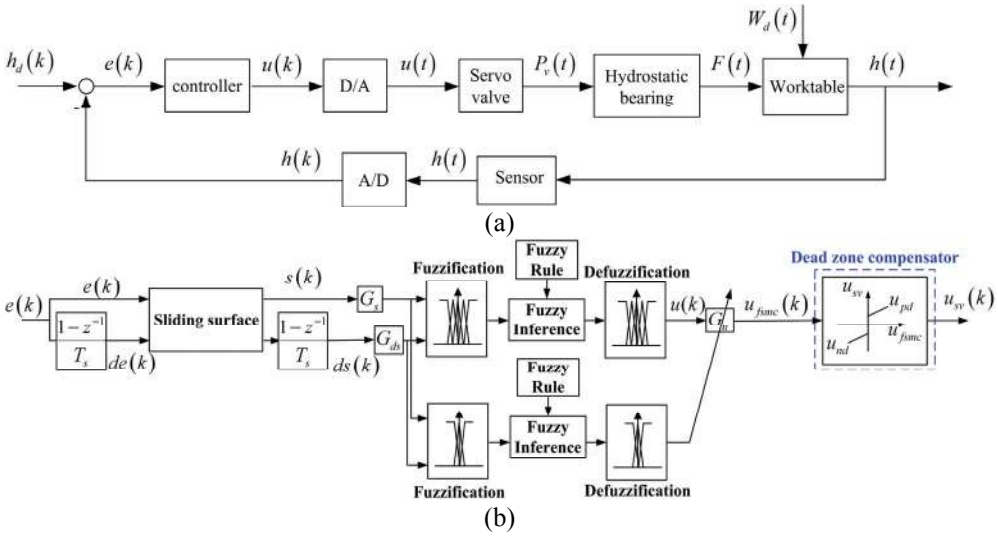

Fig. 16 (a) Block diagram of the active compensating hydrostatic bearing control system (b) Block diagram of the proposed controller ST-FSMC

Figure 16(a) shows the block diagram of the oil film thickness with the active compensating hydrostatic bearing. The objective of this control system is maintaining a constant oil film thickness of the designed hydrostatic bearing. Fig. 16(b) shows the block diagram of the Self-Tuning Fuzzy Sliding Mode Controller (ST-FSMC) with dead zone compensator. The proposed controller scheme is comprised of three parts: the fuzzy sliding mode controller, the self-tuning mechanism and the dead zone compensator, the details are as follows:

4.1 Fuzzy sliding mode controller

A classical controller requires the mathematical model of the system to be controlled. However, the Fuzzy Logic Controller (FLC) does not require such a model since it is rule-based. Therefore, the FLC has an advantage over the classical controller when it is applied to ill-defined and complex systems. The FLC includes fuzzification inference, fuzzy rule table, decision logic and defuzzification. The fuzzy rule table is dependent on error e and error rate $\dot{e}$ that complicate both membership functions and fuzzy rules. For sliding mode control, the state-space of the linear system using hydrostatic bearing model can be shown in Eq. (14). Therefore, the sliding surface s and the derivative of sliding surface $\dot{s}$ are defined as

$$s = \dot{e} + \alpha e = \left(\dot{h}_d - \dot{h}\right) + \alpha\left(h_d - h\right) = \begin{bmatrix} -\alpha & -1 \end{bmatrix} \mathbf{x} = \mathbf{C} \cdot \mathbf{x} \tag{22}$$

$$\dot{s} = \mathbf{C} \cdot \dot{\mathbf{x}} = \mathbf{C}\left(\mathbf{F}\left(\mathbf{x}(t)\right) + \mathbf{B}u(t) + \mathbf{G}W_d(t)\right) \tag{23}$$

where α is the slop of sliding surface, h_d is desired oil film thickness of the bearing, $\mathbf{CB} = \left(A_e / M\right) > 0$, and $\mathbf{CG} = \left(1/M\right) > 0$. After that, consider the reaching stability condition ($\dot{V} = s\dot{s} < 0$) which is based on the Lyapunov function ($V = s^2/2$). Then, the Lyapunov stability condition as

$$\dot{V} = s\dot{s} < -\sigma|s| \Rightarrow \lim_{k\to 0} s(k)\cdot ds(k) < 0 \tag{24}$$

Therefore, a fuzzy logic controller base on the sliding mode stability condition is designed. The membership functions can be described that are shown in Fig. 17. The output and input membership functions are normalized in the interval [-1, 1]. The FSMC rule table is listed in Table 2. The controller output signal u_{fsmc} can be defined as

$$u_{fsmc}(k) = U(k) \times G_u(k) \tag{25}$$

where $U(k)$ and $G_u(k)$ denote the controller output and output scaling factor of the controller at time instant kT, if the unit time is T.

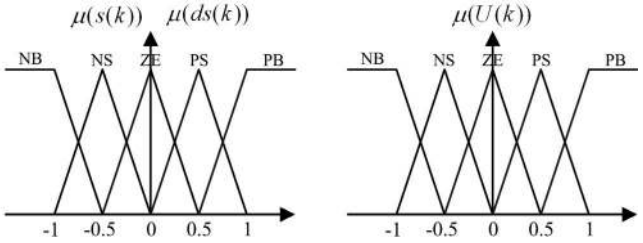

Fig. 17 Diagram of membership functions

Table 2 Rule table of FSMC

	U				
	s = NB	*s* = NS	*s* = ZE	*s* = PS	*s* = PB
ds = NB	PB	PB	PS	PS	ZE
ds = NS	PB	PS	PS	ZE	NS
ds = ZE	PS	PS	ZE	NS	NS
ds = PS	PS	ZE	NS	NS	NB
ds = PB	ZE	NS	NS	NB	NB

If the control U can be selected to satisfy the stability condition, the system will converge to the sliding surface. According to the above method, the sliding control law can be implemented with fuzzy logic by using this relation to satisfy the stability condition. There are two extreme conditions should be satisfied.

1. If $s > 0$, decreasing U value for decreasing ds to satisfy the stability condition ($s\dot{s} < 0$).

2. If $s < 0$, increasing U value for decreasing ds to satisfy the stability condition ($s\dot{s} < 0$).

4.2 Self-tuning mechanism and dead zone compensator

Because of the fixed output scaling factor G_u of FSMC doesn't have adaptability; a self-tuning mechanism is described in this section. This controller includes another fuzzy logic controller, which adjusts the output scaling factor of FSMC. The self-tuning output scaling factor can be written as

$$G_u(k+1) = G_u(k)\cdot(1+\alpha(k)) \tag{26}$$

where α is the real-time gain factor. The value of real-time gain factor is computed on-line using a model independent fuzzy rule table defined by the sliding surface s and the derivative of sliding surface $\dot{s}$ of the controlled variable. The triangular membership

functions are used for the fuzzification of the input and output variable are shown in Fig. 18. The fuzzy rule table is illustrated in Table 3.

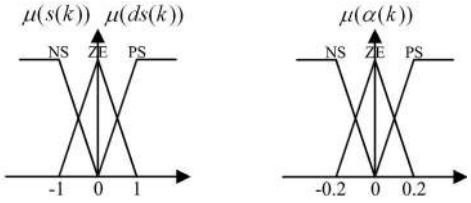

Fig. 18 Membership functions of self-tuning mechanism

Table 3 Rule table of self-tuning mechanism

	α		
	s = NS	s = ZE	s = PS
ds = NS	ZE	NS	ZE
ds = ZE	PS	ZE	PS
ds = PS	ZE	NS	ZE

Finally, the dead zone compensator can be designed to avoid the insensitive area of a servo valve. The algorithm of control voltage with dead zone compensator can be expressed by the following equation:

$$u_{sv} = \begin{cases} u_{fsmc} + u_{pd}, & if\ u_{fsmc} > 0 \\ u_{fsmc} - u_{nd}, & if\ u_{fsmc} < 0 \end{cases} \tag{27}$$

where u_{pd} is the positive compensation signal of dead-zone and u_{nd} is the negative compensation signal of dead-zone. Fig. 19 shows the real driven signal after compensation.

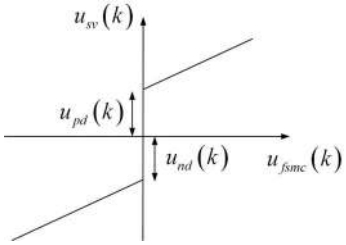

Fig. 19 The signal u_{sv} after compensation

5. Experimental Results

The dynamic test stand was built as shown in Fig. 20, to evaluate the control performance of the active compensating hydrostatic bearing. The hydrostatic bearing, hydraulic cylinder, servo valve, proportional electro-hydraulic relief valve, and the directional valve were installed on the test stand. As shown in Fig. 20, the oil film thickness between the hydrostatic bearing and oil return base was measured using non-contact displacement (range: 1mm; accuracy: 0.5μm) to feedback. The load capacity of the hydrostatic bearing was measured by the load cell (rated capacity: 20kN). To adjust the external load, a proportional relief valve (pres. adj. range: 8-140 bar) was set between the power unit and the hydraulic cylinder to regulate the pressure. Besides, to adjust the oil film thickness by regulating the pressure, a servo valve (pres. adj. range: 0-70 bar; Bandwidth: 100 Hz) was set between the power unit and the hydrostatic bearing. The flow rate was measured using flowmeter.

Figure 21 shows the static performance characteristics of the experimental results and simulations on load capacities and flow rates. It can be seen that the present experimental results for the static performance characteristics of the designed hydrostatic bearing agree well with simulation results.

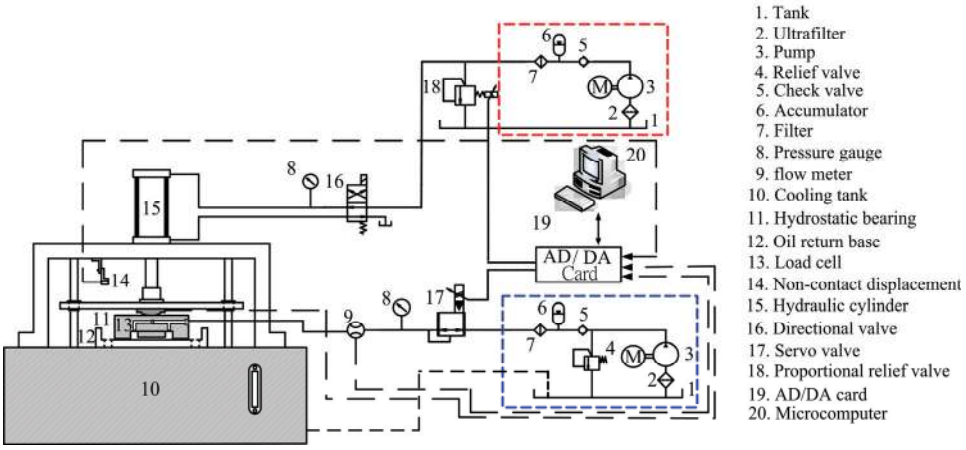

(a)

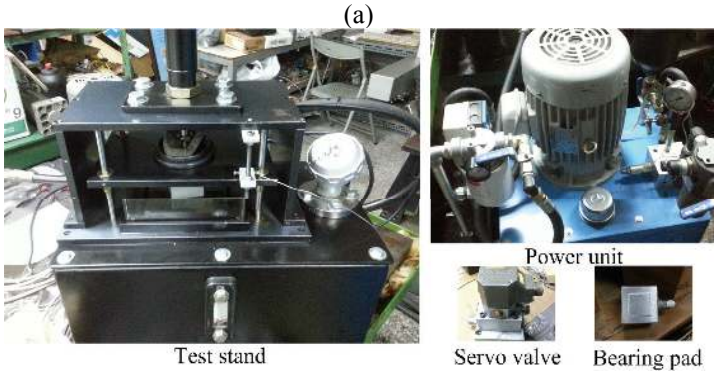

(b)

Fig. 20 Experimental apparatus for hydrostatic bearing (a) schematic diagram and (b) photograph

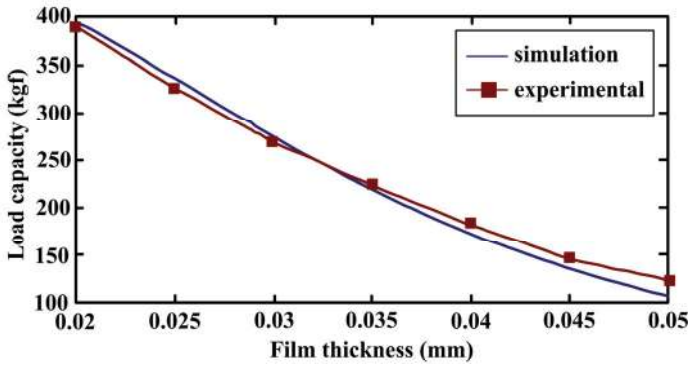

(a)

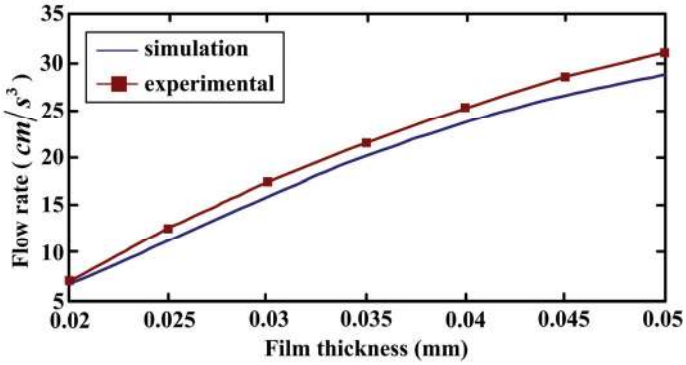

(b)

Fig. 21 Comparison of simulation and experimental results on (a) load capacity and (b) flow rate

Figure 22(a) shows a variable loading response by using the hydraulic cylinder and proportional electro-hydraulic relief valve. Fig. 22(b) shows the dynamic behavior of the experimental results. It can be seen that the designed bearing have less influence of the oil film thickness than referenced bearing. The initial oil film thicknesses for the referenced and proposed bearing are different. Because of the load capacities are different. The load capacity of the proposed design is better than referenced hydrostatic bearing. Therefore, the referenced bearing needs a thinner the oil film thickness to withstand the external load. Thus, it can be shown that the dynamic behavior of the designed bearing has strong performance.

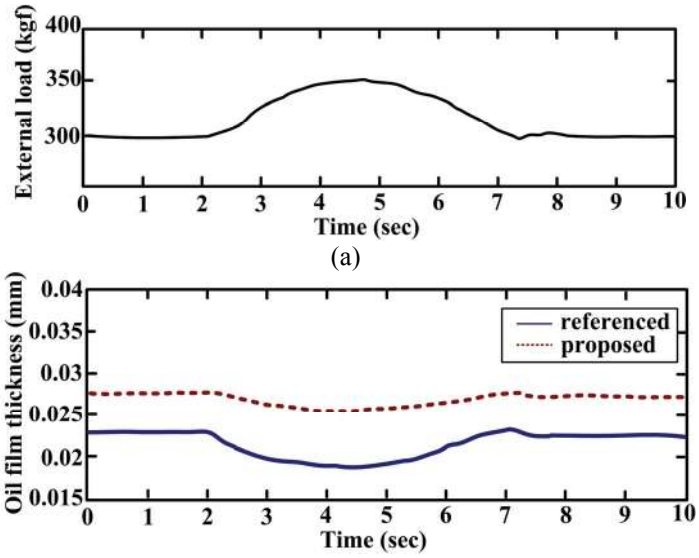

Fig. 22 (a) external load disturbance and (b) comparison between the referenced and the proposed hydrostatic bearing

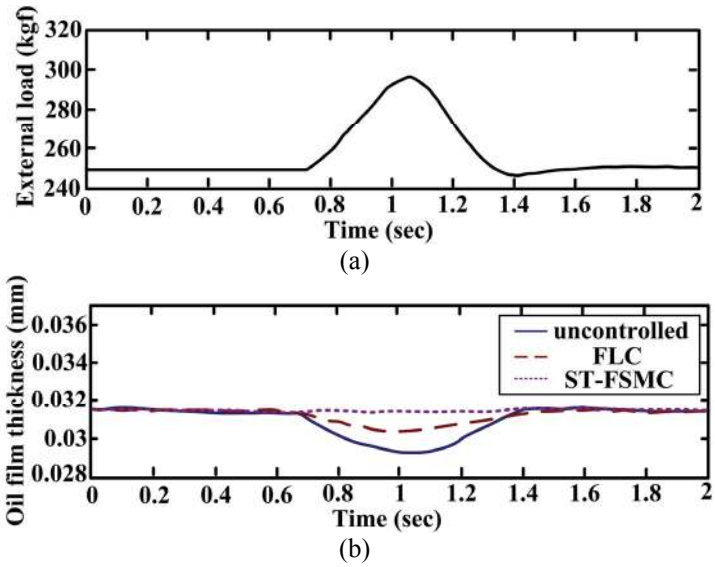

Fig. 23 (a) External load and (b) effect of different controllers for a designed hydrostatic bearing on dynamic behavior under external load

This section shows the results of the experiment conducted on an active compensating hydrostatic bearing system using a servo valve to show the effect of the proposed controller on oil film thickness consistency. Performance comparisons were conducted among the proposed controller, a fuzzy logic controller and the passive hydrostatic bearing

(uncontrolled). Fig. 23(a) shows the external load, which includes the worktable weight, the workpiece weight and the cutting force. Fig. 23(b) shows the responses of the proposed controller, the fuzzy logic controller, and the passive hydrostatic bearing as measured by time domain. To maintain constant oil film thickness, the proposed controller improves the worktable position by 78 %, and the FLC develops it by 52 %. Therefore, according to the above results, it can be seen that the ST-FSMC has the least variation on the oil film thickness of a designed hydrostatic bearing. The reason is that the ST-FSMC has more consider the sliding mode stability condition and the dead zone compensator than the others, by those additional mechanisms can effectively enhance the response of the controller to suppress the change of loads on the table.

6. Conclusion

This study aimed to optimum design of recess shape for the hydrostatic bearing and dynamic control of the oil film thickness for an active compensating hydrostatic bearing by adopting a hybrid controller with the self-tuning fuzzy sliding mode controller. The conclusions of this study are as follows:

(1) The similarity between the simulation and experimental results confirm the designed bearing has a strong static performance by using HTGA/Gray approach. It also can be shown that the designed bearing provides a uniform pressure distribution in the surface successfully.

(2) The hydrostatic bearing was actively compensated by a servo valve to maintain a constant oil film thickness. The experimental result shows the active hydrostatic bearing (controlled) is significantly better than passive one (uncontrolled). These results show that the concept of a hydrostatic bearing with hydraulic servo control technology is feasible even if the load changes.

(3) Based on the oil film thickness, the improvement rate achieved for the passive hydrostatic bearing with the proposed controller (STFSMC) at RMS is 26 % more than that with the FLC. The RMS values of the oil film thickness control using the proposed controller and FLC are 0.5μm and 1.2μm , respectively. This indicates that adopting the active compensating hydrostatic bearing associated with the proposed controller can efficiently suppress the external loads of the table.

Acknowledgements

This research was partially supported by the National Science Council of the Republic of China government under the contract no. NSC-100-2221-E-006-268.

References

(1) O'Donoghue, J. P., Rowe, W. B. and Hooke, C. J. Design of Hydrostatic Bearing Using An Operating Parameter. *Wear*, Vol. 14, No. 5 (1969), pp. 355-362.

(2) Rowe, W. B., O'Donoghue, J. P. and Cameron, A. Optimization of Externally Pressurized Bearings for Minimum Power and Low Temperature Rise. *Tribology*, Vol. 3, No. 3 (1970), pp. 153-157.

(3) Ghosh, M. K. and Majumdar, B. C. Design of multirecess hydrostatic oil journal bearings, *Tribology International*. Vol. 13, No. 2 (1980), pp. 73-78.

(4) Franchek, N. M. and Childs, D. W. Experimental test results for four high-speed, high-pressure, orifice-compensated hybrid bearings. *ASME Journal of Tribology*, Vol. 116, No. 1 (1994), pp. 147-53.

(5) Sharma, S. C., Jain, S. C. and Bharuka, D. K. Influence of Recess Shape on the Performance of a Capillary Compensated Circular Thrust Pad Hydrostatic Bearing. *Tribology International*, Vol. 35, No. 6 (2002), pp. 347-365.

(6) Sharma, S. C., Sinhasan, R. and Jain, S. C. Performance characteristics of multirecess hydrostatic/hybrid flexible journal bearing with membrane type variable-flow restrictor as compensating elements. *Wear*, Vol. 152, No. 2 (1992), pp. 279-300.

(7) Singh, N., Sharma, S. C., Jain, S. C. and Reddy, S. S. Performance of membrane compensated multirecess hydrostatic/hybrid flexible journal bearing system considering various recess shapes. *Tribology International.* Vol. 37, No. 1 (2004), pp. 11-24.

(8) Yakir, E. M. Regulators for Open Hydrostatic Slideways. *Machines and Tooling*, Vol. 44, No. 8 (1973), pp. 28-32.

(9) Bushuyev, V. V. Angular Stiffness of Hydrostatic Slides. *Machines and Tooling*, Vol. 124, No. 10 (1973), pp. 26-29.

(10) Wang, C. and Cusano, C. Dynamic Characteristics of Externally Pressurized, Double-Pad, Circular Thrust Bearings with Membrane Restrictors. *ASME Journal of Tribology*, Vol. 113, No1 (1991), pp. 158-165.

(11) Ingert, G. Kh. and Lur'e, B. G. Dynamic Stiffness of Open-Circuit Hydrostatic Slideways With Slotted-Spring Regulators. *Machines and Tooling*, Vol. 47, No. 2 (1976), pp. 31-33.

(12) Rippel, H. C. Design of Hydrostatic Bearings：Part 2—Controlling Flow with Restrictors. *Machine Design*, August 15 (1963), pp. 122-126.

(13) Rippel, H. C. Design of Hydrostatic Bearings：Part 3—Influence of Restrictors on Performance " , *Machine Design*, August 29, (1963), pp. 132-138.

(14) Hesselbach, J. and Abel-Keilhack, C. Active hydrostatic bearing with magnetorheological fluid. *Jouranl of Applied Physics*, Vol. 93, No. 10 (2003), pp. 8441-8443.

(15) Munzinger, C., Weis, M. and Herder, S. Smart adaptronic hydrostatic guiding system for machine tool slides. *Proceedings of SPIE*, Vol. 7288 (2009), pp. 1-3.

(16) Shao, J. P., Han, G. H. Zhang, Y. Q., Dong, Y. H. and Li, H. M. Hardware-in-loop simulation on controllable hydrostatic thrust bearing. *Proceedings of the IEEE International Conference on Automation and Logistics*, (2008), pp. 1095-1099.

(17) Han, G. H., Shao, J. P., Qin, B. and Dong, Y. H. Hardware-in-loop simulation on hydrostatic thrust bearing worktable pose. *Journal of Central South University of Technology*, Vol. 5 (2008), pp. 250-256.

(18) Tsai, J. T., Liu, T. K. and Chou, J. H. Hybrid Taguchi-Genetic Algorithm for Global Numerical Optimization. *IEEE Transactions on evolutionary computation*, Vol. 8, No. 4, (2004), pp. 365-377.

(19) Kuo, Y., Yang, T., and Huang, G. W. The use of a grey-based Taguchi method for optimizing multi-response simulation problems. *Taylor & Francis*, Vol.40, No.6 (2008), pp. 517-528.

(20) Hwang, G. C. and Lin, S.C. Stability approach to fuzzy control design for nonlinear systems. *Fuzzy Sets and Systems*, Vol. 48, No. 3 (1992), pp. 279-287.

(21) Li, T. H. S. and Shieh, M. Y. Switching-type fuzzy sliding mode control of a cart-pole system. *Mechatronics*, Vol. 10, No. 1-2 (2000), pp. 91-109.